Intraseasonal Oscillations in the Global Atmosphere. Part II: Southern Hemisphere

MICHAEL GHIL

Climate Dynamics Center, Department of Atmospheric Sciences, and Institute of Geophysics and Planetary Physics, University of California, Los Angeles, California

KINGTSE MO

Climate Analysis Center, National Meteorological Center, Washington, DC

(Manuscript received 7 November 1989, in final form 1 October 1990)

ABSTRACT

In Part II of this two-part article, we complete the systematic examination of oscillatory modes in the global atmosphere by studying 12 years of 500 mb geopotential heights in the Southern Hemisphere. As in Part I, for the tropics and Northern Hemisphere extratropics, the data were band-pass filtered to focus on intraseasonal (IS) phenomena, and spatial EOFs were obtained. The leading principal components were subjected to singular spectrum analysis (SSA), in order to identify nonlinear IS oscillations with high statistical confidence.

In the Southern Hemisphere, the dominant mode has a period of 23 days, with spatial patterns carried by the second and third winter EOF of the IS band. It has a zonal wavenumber-four structure. The 40-day mode is second, and dominated by wavenumbers three and four, while a 16-day mode is too weak to separate its spatial behavior from the previous two. The IS dynamics in the Southern Hemisphere is more complex and dominated by shorter wavenumbers than the Northern Hemisphere. No statistically significant correlations between the Southern Hemisphere and the tropics or the Northern Hemisphere are apparent in the IS band.

1. Introduction

Low-frequency variability (LFV) of the Southern Hemisphere, like other aspects of its atmospheric circulation and dynamics, has been studied less intensely than for the tropics or Northern Hemisphere extratropics. In the intraseasonal (IS) band, persistent anomalies have been documented by Trenberth (1985) and by Trenberth and Mo (1985), and classified into multiple flow regimes by Mo (1986), while Mo and Ghil (1987) and Vautard et al. (1990) introduced Markov chains to describe the transitions between these regimes. Here we investigate the oscillatory part of IS behavior in the Southern Hemisphere troposphere.

Branstator (1987) found a weak manifestation of his 23-day westward-traveling wave in Southern Hemisphere (SH) data, as part of a global nine-year analysis. Knutson and Weickmann (1987) found that fairly persistent anomalies of the streamfunction field at 250 mb develop within the 30–60 day band in a few preferred locations, during SH winter. Limited evidence of eastward propagation during winter, and very weak activity during the SH summer were found by these authors. Intraseasonal variability in the SH winter stratosphere was studied by Mechoso et al. (1991).

Corresponding author address: Prof. Michael Ghil, Dept. of Atmospheric Sciences, University of California, 405 Hilgard Avenue, Los Angeles, CA 90024-1565.

In Ghil and Mo (1991, Part I hereafter), we carried out a systematic examination of IS oscillations in the tropics and Northern Hemisphere (NH) extratropics, by projecting spatial patterns onto leading empirical orthogonal functions (EOFs) and studying the temporal behavior of the corresponding principal components (PCs) by singular spectrum analysis (SSA), as well as by classical spectral methods. The same systematic approach is applied to SH data in Part II here.

In section 2, we present the dataset and summarize the statistical methods. Section 3 contains the EOF patterns, and section 4 the SSA results. Standing- and traveling-wave features are documented in section 5, followed by concluding remarks in section 6.

2. Data and methods

The SH dataset consists of once-daily 500 mb heights from the World Meteorological Center in Melbourne, Australia. It covers the period from June 1972 to September 1984, and is on a 4° latitude × 5° longitude rectangular grid from 10°S to 90°S.

a. Filtering and EOF analysis

The grand time mean, as well as the annual and semiannual cycle, calculated as the two harmonics with the corresponding periods, were removed at each grid point. The resulting daily anomalies were band-pass

filtered to yield half-power points at 10 and 120 days, as described in Part I. Two other IS bands, from 10 to 90 days and from 10 to 150 days, were also used for verification purposes.

EOF analysis was carried out for the entire time series, as well as for the summer and winter seasons separately. The time mean of the given data subset was removed for each seasonal analysis. The data were standardized at each point in space by the variance in time. EOF analysis was then performed on a grid with nearly-equal spacing (Barnston and Livezey 1987), yielding 371 points.

b. Singular spectrum analysis (SSA)

SSA is a statistical technique related to EOF analysis, but applied in the time domain, rather than the spatial domain. It is used extensively in signal processing (Pike et al. 1984).

Given a uniformly sampled, zero-mean time series $x_i = x(t_0 + i\Delta t)$ of length N_T, one considers its lagged autocovariance matrix **C** up to lag $M\Delta t$. The eigenvalue–eigenvector decomposition of **C** gives eigenvalues λ_k, whose square roots are the singular values (hence SSA), and EOFs $\rho_k(s_j)$, as well as the corresponding PCs, in a way analogous to spatial EOF analysis. To prevent confusion, we shall call the latter S-EOFs and S-PCs, and the former T-EOFs and T-PCs. The T-PCs are still functions of time, $t_i = t_0 + i\Delta t$, like the S-PCs, but the T-EOFs are functions of lag, $s_j = j\Delta t$, rather than of space (see Appendix A of Part I for details). Each T-PC has variance λ_k, in decreasing order, and it represents a filtered version of the time series $x(t_i)$, the filter being a weighted moving average with weights $\rho_k(s_j)$. The T-PCs are mutually uncorrelated at zero lag.

SSA was introduced into nonlinear dynamics by Broomhead and King (1986) and by Fraedrich (1986). It was further refined in this context and applied to climatic time series by Vautard and Ghil (1989). The latter authors explored in particular the relation with usual spectral analysis, and showed that narrow peaks on a broadband background will appear as pairs of singular values in SSA. The associated T-PCs are in quadrature with each other.

The advantage of SSA over other types of spectral analysis is that the filters ρ_k are not prescribed a priori, but are determined, optimally, from the data themselves. Hence SSA is well suited to detect and analyze weak oscillations in a noisy system. In particular, the T-EOFs need not be sinusoidal, and thus the method does not need to decompose a single, intrinsically nonlinear oscillation into a large number of sine waves. SSA will exhibit such an oscillation as a single pair of EOFs, along with the appropriate variance, which equals the mean amplitude squared.

A more detailed description of SSA is given in Appendix A of Part I, where it is also shown that band-pass filtering does not produce spurious pairs of T-EOFs out of basically red time series. Further applications of SSA in the meteorological literature are given by Rasmusson et al. (1990).

3. EOF patterns

The S-EOF analysis in the IS band was performed using 500 mb heights for summer and winter seasons separately. There are 13 winters and 12 summers of data available and we use 120-day seasons. Taking 20 days as the decorrelation time, there are 78 degrees of freedom for the EOF analysis in each season. The first six S-EOF patterns for the SH winter appear in Figs. 1a–f.

The first EOF consists of 6.5 ± 1.0% of the total variance, and it resembles very well the leading EOF of daily maps in Fig. 12a of Mo and Ghil (1987). It is dominated by zonal wavenumbers one and three and exhibits a strong phase reversal between high and low latitudes. The second and third EOFs consist of 5.1 ± 0.8% and 4.8 ± 0.8% of the total variance respectively, and are not well separated statistically. Both EOFs show a wavenumber-four pattern (compare Farrara et al. 1989, Fig. 1) and they are in zonal quadrature with each other. Composites of positive and negative extremes of the two S-PCs (not shown) indicate that this pair represents an eastward-traveling wave.

EOF 4 consists of 4.05 ± 0.6% of the total variance, and has a mixture of wavenumbers four and five at high and low latitudes, respectively. EOF 5 consists of 3.4 ± 0.5% of the total variance and has a wavenumber-five pattern throughout. EOF 6 consists of 3.2 ± 0.5% of total variance and it shows a wavetrain from Tierra del Fuego to Tasmania; its equivalent wavenumber is six.

A break occurs in the partial variance curve after the fourth EOF. The combined IS variance of the first four EOFs here is 20.5%, compared to 29.1% for the first four NH EOFs (Table 1 of Part I). This indicates clearly the greater complexity of SH large-scale dynamics, with a much larger role for zonal wavenumbers four, five and six, reflected in SH winter EOFs two-through-six.

In the summer season, the first EOF has the same pattern as Fig. 1a. EOFs 2 and 3 both show a wavenumber-five pattern and are in zonal quadrature with each other. Wavenumber-four patterns appear now as EOFs 4 and 5. Both patterns, of wavenumbers four and five, represent eastward-traveling waves. In both SH summer and winter, EOF patterns in the IS band show patterns with wavenumbers three, four and five. The order of importance of the three dominant patterns and their percentages of variance may differ from one season to the other, but nevertheless they are present in both. This is different from the situation for NH EOF patterns, which show larger seasonal variation.

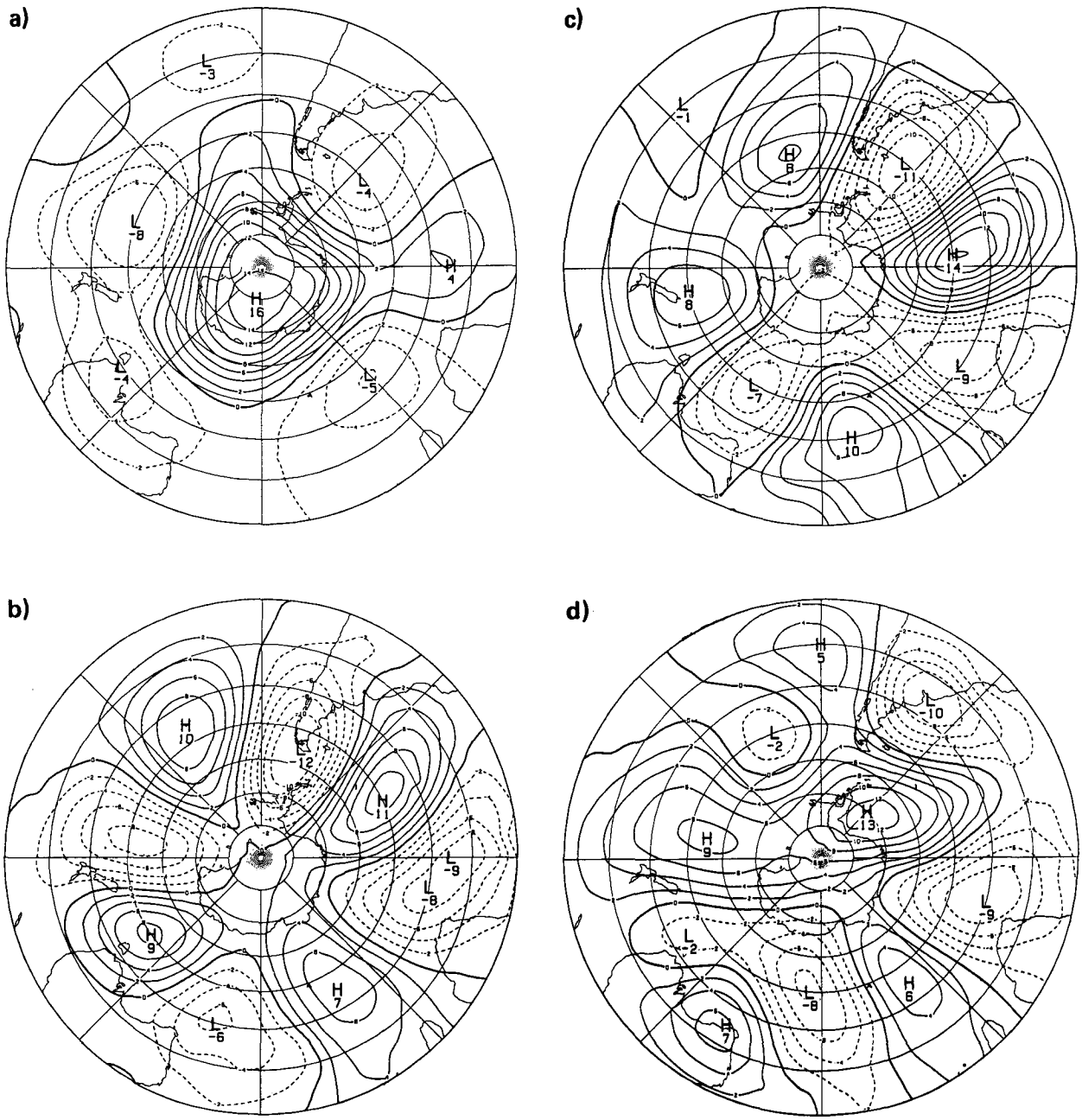

FIG. 1. The S-EOFs of IS-filtered 500 mb heights. (a) EOF 1, (b) EOF 2, (c) EOF 3, (d) EOF 4, (e) EOF 5, and (f) EOF 6 for the SH winter. EOFs are normalized to unit vector length × 100; negative contours (dashed), zero contour (heavy solid) and positive contours (light solid); contour interval is 2.

Only one pattern (Fig. 2d of Part I) appears in all seasons in the NH data.

The importance of intermediate-scale waves, with zonal wavenumbers 4–7, in the upper troposphere and lower stratosphere of the Southern Hemisphere was discovered by Kalnay-Rivas et al. (1981), and confirmed by Salby (1982) and by Hamilton (1983). Salby emphasized the dominance of the "pentagonal" wave during the SH summer of 1979, and its eastward-traveling character, with a period near 10 days. But a standing component of this wave, within the 8-15 day band, is also apparent in his work (Salby 1982, Fig. 9). Randel and Stanford (1983) review the information on the pentagonal and adjacent waves, including references to some preliminary observations from the early and mid-1970s. Randel and Stanford substantiate

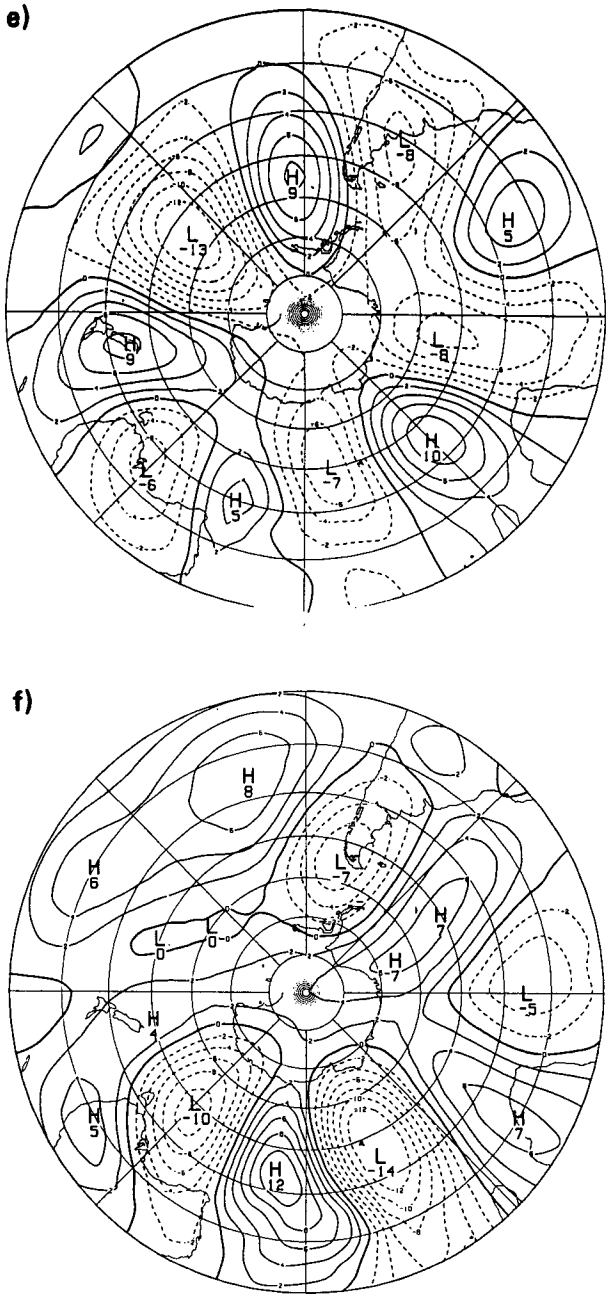

FIG. 1. (*Continued*)

the equivalent-barotropic character of the intermediate-scale waves, and illustrate the interaction between the zonal-mean flow and the pentagonal wave (their Fig. 8), and between the standing and traveling components of this wave (their Fig. 7).

4. SSA results

Since there is little seasonal variation in the S-EOF patterns, all 500 mb height data were projected onto the winter EOFs, and SSA analysis performed on the first five IS-filtered S-PCs. Window sizes of $M = 40$, 60 and 80 were used, as explained in Part I. The first three pairs of T-PCs are stable and independent of window size for all five leading S-PCs. SSA results are given in Table 1 for $M = 60$, listing for each pair the combined percentage of total variance and the period of the corresponding oscillation. The results listed are for a 10–120 day band-pass window (see Fig. 1 of Part I), but calculations were repeated for 10–90 and 10–150 day windows. None of the modes listed in the table, except the first pair of T-PCs for S-EOF 1, changes substantially.

The SSA spectra of each leading S-PC in the Southern Hemisphere are flatter ("redder") than in the Northern Hemisphere and in the tropics; pairs of T-PCs are less markedly separated here than in Part I, but still significantly so. There are two clear groupings of periods, familiar from Part I, 36–40 days and 21–26 days, with a much weaker 16-day period. We call the leading two oscillations S40 and S23. The first pair of T-PCs for S-EOF 1, with a period of 64 days, is probably due to the band-pass filtering (compare Appendix A of Part I). Its period shifts to 50 days when using a 10–90 day band, while the period of the other pairs is not affected (only their respective variances change slightly in the narrower and broader bands).

As explained in Part I, in addition to near-equality of the variances, another criterion for a pair of T-PCs to represent a genuine oscillation, rather than a sampling accident, is a very high lagged cross-correlation between the two, at a lag close to one quarter of the period. The maximum cross-correlations (compare Tables 2 and 4 of Part I), for the first pair of T-PCs of S-PCs 2, 3 and 5 are above 0.90, and 0.85 in the case of S-EOF 4. The number of degrees of freedom for testing these cross-correlations, according to Eq. (3.3) of Part I (see also Sciremammano 1979), is $n_d \approx 30$, yielding a threshold value for the 95% confidence level of about 0.37. The maximum cross-correlation for the second pair of T-PCs in Table 1 is about 0.74. The only cross-correlation for a third pair significant at this level is for S-EOF 2.

We saw that in the NH IS data the N45 mode is dominant over N21 by a factor of 2.4:1.0 (Table 2 of Part I). In the tropics T48 is dominant in the convectively active Indian–western Pacific sector, while both T48 and T28 are equally important in the less active and smaller eastern Pacific sector (Table 5 of Part I). In the SH data, the S23 mode is favored. S23 is present in the first pair of T-PCs for S-EOFs 2 and 3, and in the second pair of T-PCs for S-EOFs 1, 4 and 5, for a combined total of 4.0% of IS variance, while S40 manifests itself through the first pair of T-PCs in S-EOFs 4 and 5 and the third pair of S-EOF 2, for a total of 1.9% of IS variance. In particular, the mere 1.9% of IS variance for S40 (cf. Table 1 here) has to be compared with the 8.6% for N45 (cf. Table 2 in Part I), while

TABLE 1. Oscillatory modes of the first five S-PCs in the IS band (10–120 days).

S-EOF	Total variance (%)	T-PCs 1 and 2 Variance** (%)	T-PCs 1 and 2 T (days)	T-PCs 3 and 4 Variance** (%)	T-PCs 3 and 4 T (days)	T-PCs 5 and 6 Variance** (%)	T-PCs 5 and 6 T (days)
1	6.5 ± 1.0	28.3 ± 3.2	64	23.1 ± 2.6	26		
2	5.1 ± 0.8	21.1 ± 2.4	21	16.2 ± 1.8	16, 30*	14.5 ± 1.6	36
3	4.8 ± 0.8	17.9 ± 2.0	21	14.5 ± 1.6	16, 30*		
4	4.0 ± 0.6	16.8 ± 1.9	40	13.5 ± 1.5	26		
5	3.4 ± 0.5	14.0 ± 1.6	36	12.4 ± 1.4	26, 60*		

* Second peak.
** The error ± $\delta\lambda_k$ in each variance $\lambda_k = \sigma_k^2$ of a T-PC is estimated by Eqs. (3.1a,b) of Part I; $M = 60$, $N_d = 78$.

S23, with 4.0% in the Southern Hemisphere, is slightly more important than N21, with 3.6% of NH variance in the IS band. The corresponding NH variances, based on the 1972–1984 time interval for which SH data are analyzed here, become 9.0% for N45 and 4.2% for N23.

This confirms the results of Knutson and Weickmann (1987) on the relative weakness of the 30–60 day oscillation in the Southern Hemisphere compared to the Northern Hemisphere, and on the relative strength of the extratropical oscillation during the winter season in either hemisphere (SSA results for SH summer omitted for the sake of brevity). The latter result suggests an independent, extratropical mechanism of the oscillation in either hemisphere, but with a similar sensitivity of its amplitude to the magnitude of the equator-to-pole temperature gradient (Ghil 1987, 1988).

We restrict therewith our attention to SH winter EOFs and their S-PCs. Singular spectra for S-PCs 2 and 5 are given in Figs. 2a,b. They are representative for all leading S-PCs of SH data. In particular, the singular spectrum of S-PC 3 (not shown) is very similar to that of S-PC 2 (Fig. 2a). The SH singular spectra have a much smaller dynamic range ($0–10^{-3}$ vs $0–10^{-7}$ for the NH spectra) and are much flatter than those for the Northern Hemisphere (Figs. 3a,b in Part I). This relative flatness is a diagnostic of the greater complexity of SH IS dynamics, which is characterized in the time domain by smaller separation between oscillatory modes, and in the spatial domain by greater significance of intermediate-scale waves.

Still, there is a change of slope in the spectra between $k \approx 25$, for $M = 40$, and $k \approx 50$, for $M = 80$. The comparable numbers are $15 \leqslant k \leqslant 30$ for $40 \leqslant M \leqslant 80$ in the case of the NH S-PCs (§3b in Part I). Counting the number of dynamically-significant S-EOFs as six, rather than as four, yields a number of degrees of freedom characterizing SH IS variability of no more than $6 \times 50 = 300$ versus $4 \times 30 = 120$ for the Northern Hemisphere. This estimate is still within the range suggested in section 6.5 of Ghil and Childress (1987), and is amenable to the thorough, detailed study of nonlinear dynamics illustrated in section 6.4 there.

The first S-EOF has a leading oscillation with a period of 64 days. Composites of four phases of this oscillation, keyed to the extrema of T-PCs 1 and 2 (not shown) indicate it to be a standing wave, dominated by zonal wavenumber one in high latitudes and wavenumber four in mid-latitudes.

Here S23 is first mode for S-EOFs 2 and 3. For S-EOF 5, there is considerable degeneracy between the

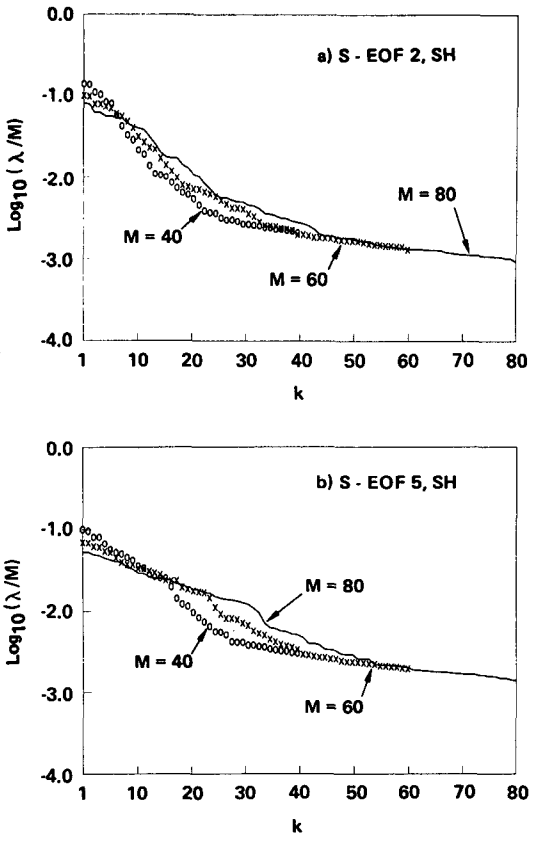

FIG. 2. Singular spectrum analysis (SSA) of (a) S-PC 2 and (b) S-PC 5. Embedding dimensions used are $M = 40(\mathrm{O})$, $60(\times)$ and $80(-)$. The singular values λ_k are normalized by M, cf. Vautard and Ghil (1989).

S40 and S23 modes. Branstator (1987) found the 23-day wave in the Southern Hemisphere to have smaller amplitude and larger wavenumbers than in the Northern one. This is not entirely consistent with our findings, S23 having a total of 4.0% of IS variance versus 3.6% for N21 in the Northern Hemisphere; the discrepancy might be due to Branstator's attempt to project his nine-year data onto global complex EOFs.

The two leading T-PCs associated with S-EOF 5 for six selected years are shown in Fig. 3. The SH 40–50 day oscillation is stronger, on average, in the hemisphere's winter than in its summer, but is even more intermittent and irregular than in the Northern Hemisphere (Figs. 6 and 7 of Part I). Considerable interannual variability is apparent, with some strong episodes in all seasons.

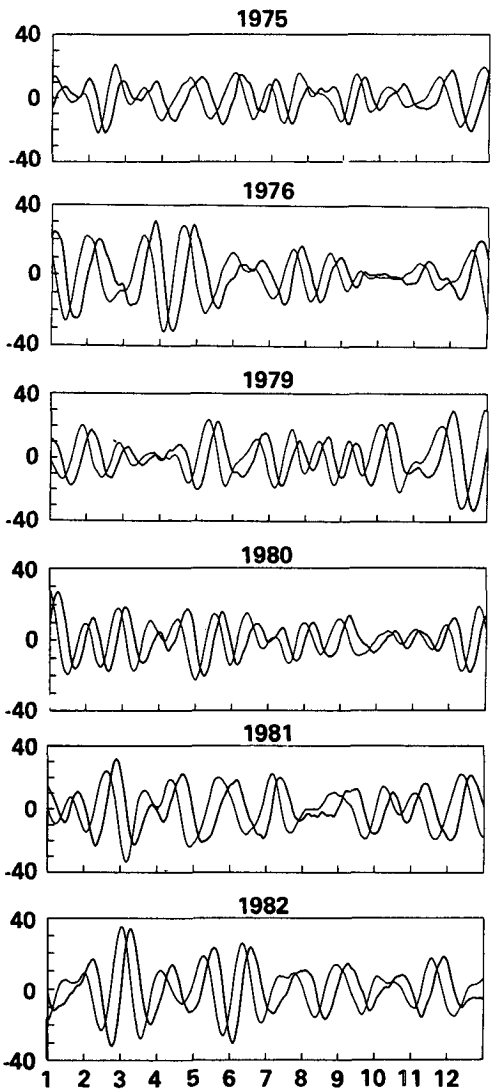

FIG. 3. The first (dark solid) and second (light solid) T-PC associated with S-EOF 5 for six selected years.

5. Standing and traveling waves

Mechoso and Hartmann (1982) studied traveling planetary waves in the SH troposphere and stratosphere using space–time spectral analysis of daily, unfiltered data for May–September 1979. They found that substantial standing components are present at 40° and 50°S in zonal wavenumbers 1, 2 and 3. Westward-moving components of wavenumbers 1 and 2 were identified with external barotropic Rossby modes, while eastward-moving components of wavenumbers one-to-four were identified with baroclinic modes.

To investigate traveling and standing waves in the IS band, we plotted Hovmöller (1949) diagrams for each SH winter at 40° and 50°S. Eastward-traveling waves seem to dominate these diagrams. Hovmöller diagrams of IS-filtered fields at 50°S for the winters of 1976 and 1979 appear in Figs. 4a,b. Eastward-traveling waves with a period of 16–25 days dominate the winter of 1976. They consist largely of wavenumbers 2 and 4. During the winter of 1979, eastward-traveling waves still dominate the picture; they have large components of wavenumbers 3 and 4, and periods of 25–36 days. A substantial standing component, with wavenumbers 1, 2 and 3 is also present. There are, in particular, time intervals where wavenumber three slows down and remains stationary for 7–10 days. These intervals correspond to quasi-stationary events dominated by this wave (Mo 1986; Mo and Ghil 1987; compare also Hartmann 1977).

To study the spatial structures of S40 and S23, we turned to composites. Since the S40 signal is much weaker in the Southern than in the Northern Hemisphere, the time series had to be filtered before compositing. Besides restriction to the IS band, as in Figs. 9 and 11 of Part I, filtering is done by projecting the time series of maps $\phi(\mathbf{r}, t)$, where $\mathbf{r}$ is the position vector, and ϕ the 500 mb height field, onto the T-PC with respect to which compositing is to be done. The filter for the time series at each grid point consists therewith, cf. Eqs. (A.3)–(A.6) of Part I, of

$$\tilde{\phi}\left(\mathbf{r}, t + \frac{M}{2}\right) = \sum_{s=1}^{M} \phi(\mathbf{r}, t + s)\rho_k(s);$$

here $\tilde{\phi}$ is the filtered field, and $M = 60$. Just as for the NH composites, we averaged over all filtered maps for those dates where the T-PC associated with a particular S-PC mode exceeds 1.8 times its own standard deviation.

The four phases of the S23 mode appear in Fig. 5. These are obtained according to T-PCs 1 and 2 of S-EOF 2. Very similar plots (not shown) result by using the two leading T-PCs of S-EOF 3, which is in zonal quadrature with S-EOF 2. The four panels show a well-defined wave, dominated by zonal wavenumber four. The four phases indicate a certain amount of motion, but do not allow us to discern a preferred direction of

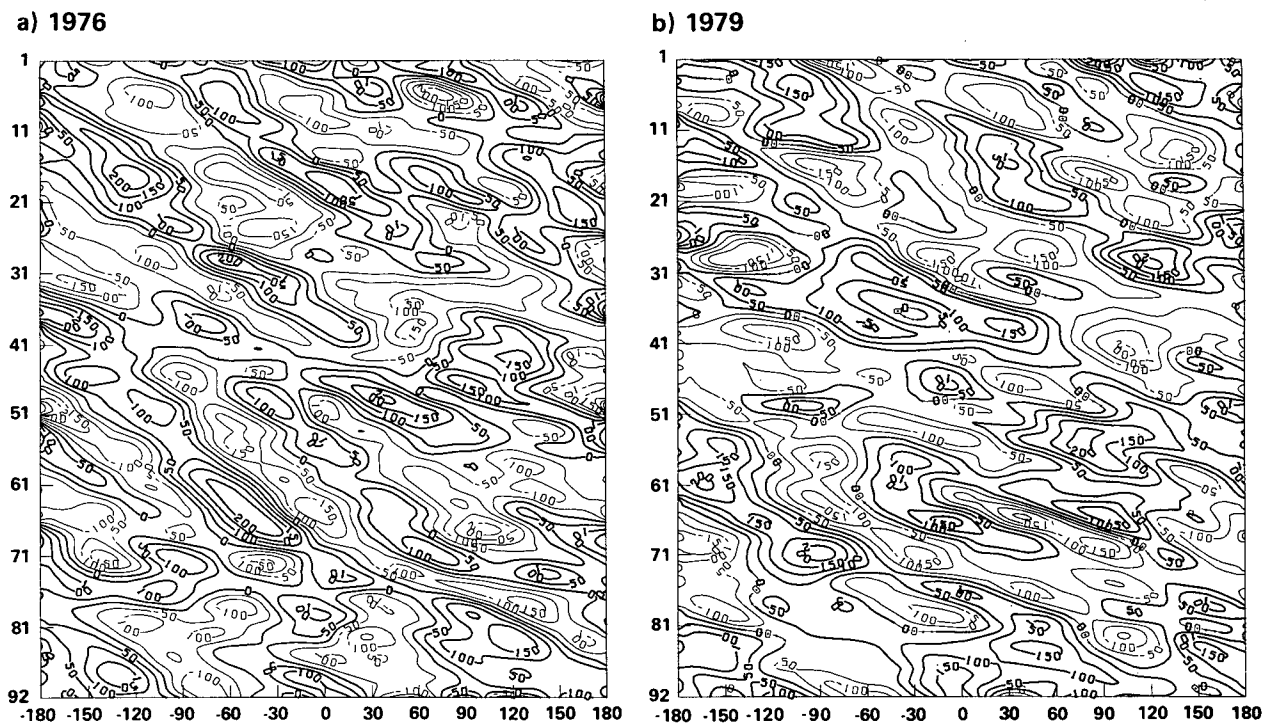

FIG. 4. Hovmöller diagrams for IS-filtered 500 mb height anomalies at 50°S for the SH winter: (a) 1976, (b) 1979.

travel. Hovmöller diagrams, however, strongly suggest that the motion is mostly eastward. In the Northern Hemisphere, the N21 wave is dominated by wavenumber two in the mid-latitudes and travels westward. It is interesting, on the other hand, that S23, like N21, has large amplitudes over and near the American continent. S23 might be related to the Pacific/South-American (PSA) stationary pattern, detected in SH data by Mo and Ghil (1987), in the same way that N21 appears to be related to the Pacific/North-American (PNA) pattern.

Figure 6 shows the four phases of the S40 mode, derived from the extrema of T-PCs 1 and 2 of S-EOF 5. Composites based on the extrema of T-PCs for S-EOF 4 yield the same patterns. Amazingly enough, while S-EOFs 4 and 5 are dominated by wavenumber five, what emerges from Figs. 6a–d is a pattern mostly containing wavenumbers three and four. Features in the Pacific sector, from Australia to South America, are much stronger than in the complementary, Atlantic–Indian sector. Wavenumber three has both traveling and standing components. The phase of S40 shown in Fig. 6c matches the composite of quasi-stationary events shown by Mo (1986, Fig. 8b) and by Mo and Ghil (1987, Fig. 11c). But the dates of the quasi-stationary events there match only partially the dates that went into Fig. 6c.

Comparison of Fig. 3 here with Figs. 6 and 7 of Part I shows poor correlation between episodes of large-amplitude 40–50 day oscillation in the two hemispheres. Cross-correlation between T-PC 1 for S40 with the corresponding segment of T-PC 1 for N45 are not significant at any lag between −20 and +20 days. Cross-correlations between time series of key points in the composite of the SH oscillation's extreme phase (Fig. 6a here) with NH key points (Fig. 14 in Part I) or with key points in the tropics (Fig. 15a and Table 5 in Part I) are not significant either.

6. Summary and discussion

Singular spectrum analysis (SSA: Vautard and Ghil 1989) provides a novel and powerful tool for the study of oscillatory phenomena in the atmosphere. Its main advantage is that the basic oscillations into which it decomposes a time series are not functions of a prescribed, harmonic form. These basic oscillations are determined, in shape as well as in variance, from the time series itself. We refer to the shape of these oscillations as temporal EOFs (T-EOFs), to the corresponding standard deviations as the singular values, and to the principal components (PCs) which provide the expansion of the time series into its T-EOFs as T-PCs. Each basic oscillation is represented by a pair of T-EOFs with nearly-equal variance, in quadrature with each other. Such a pair corresponds to the sine and cosine of the same frequency in a Fourier expansion, but the point is precisely that the T-EOFs differ in shape

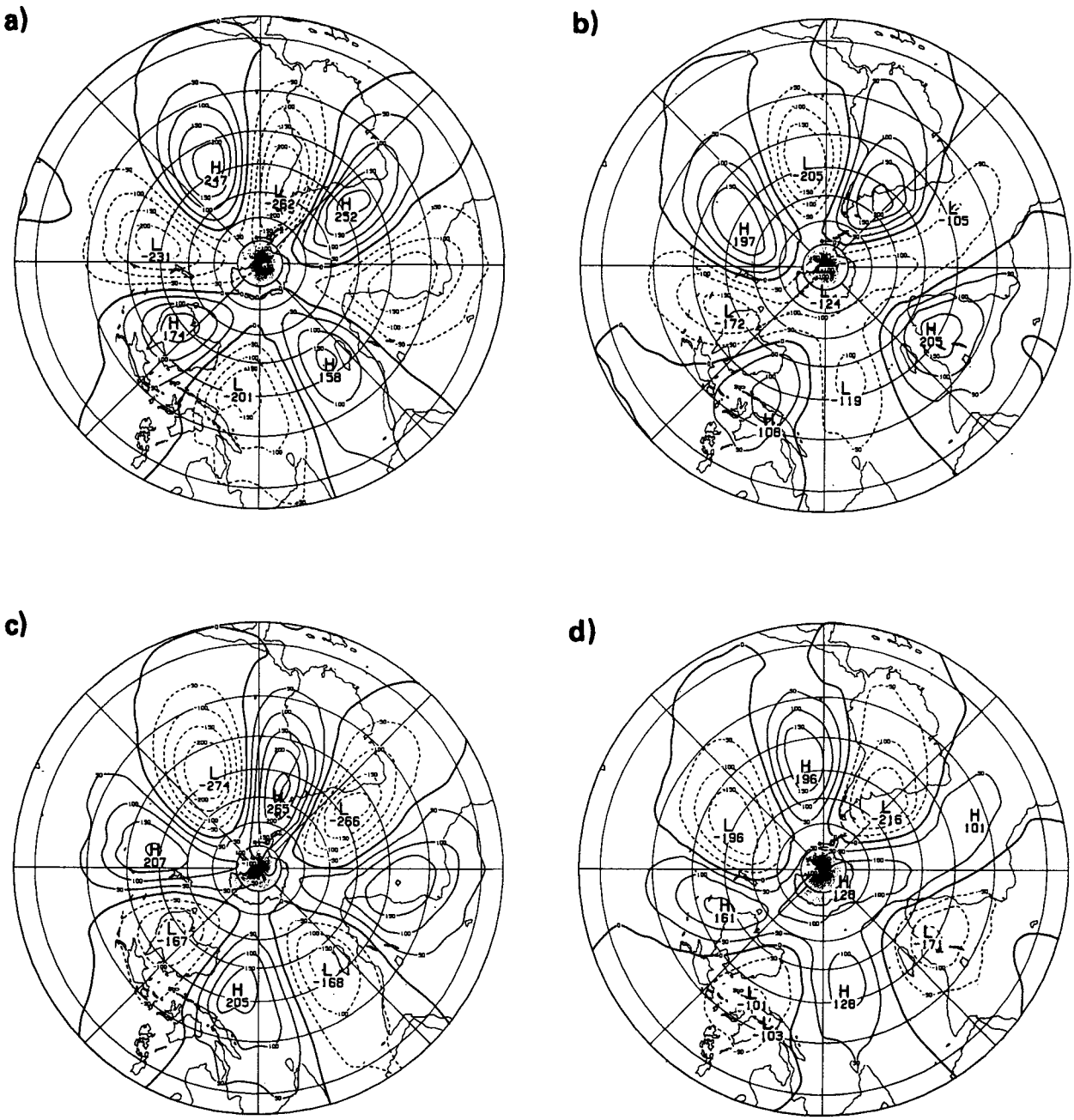

FIG. 5. Composite of filtered (see text for details) 500 mb anomalies for T-PCs of S-PC 2. (a) Positive phase of T-PC 1; (b) positive phase of T-PC 2; (c) negative phase of T-PC 1; and (d) negative phase of T-PC 2. Contour interval is 50 m.

from trigonometric functions, and that they are naturally ordered by the associated variance, rather than by frequency.

Together with the classical tools of spatial EOF analysis, multiple time series analysis in the time and spectral domain, Hovmöller diagrams and compositing, we applied SSA to the longest continuous record of daily maps in the Southern Hemisphere. These statistical tools complemented each other to reveal a number of oscillatory features in the intraseasonal (IS) band, which present both similarities with and differences from those found in Part I for the tropics and Northern Hemisphere (NH) extratropics.

In the Southern Hemisphere, the 21–26 day mode, which we called S23, is strongest. Its flow pattern is carried mostly by spatial EOFs (S-EOFs) 2 and 3, which

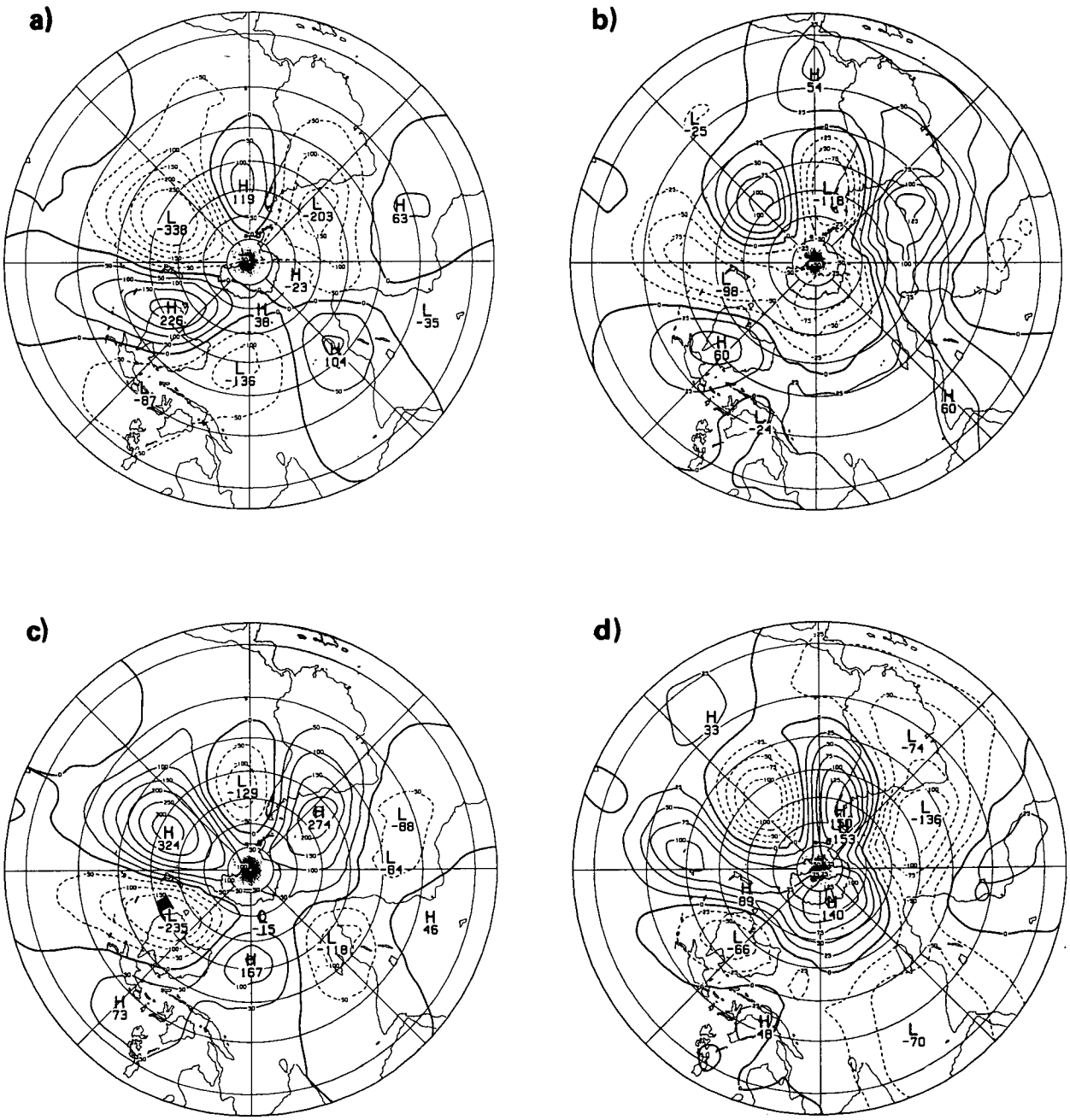

FIG. 6. As in Fig. 5, but for S-PC 5.

are in zonal quadrature with each other. S23 is dominated by an eastward-traveling wavenumber four in midlatitudes and contains at least 4.0% of the IS variance. In our NH data, the N21 mode had only 3.6% of the IS variance and, like the Branstator (1987) and Kushnir (1987) wave with which it can be identified there, was dominated by a westward-traveling wavenumber two in midlatitudes.

Both N21 and S23 have their largest amplitude near the American Continent. This suggests that the Pacific/South American (PSA) pattern of Mo and Ghil (1987) plays the same role in giving rise to, or modulating, the S23 mode as the PNA pattern plays for the N21 mode.

The 36–40 day mode which we called S40 is carried mostly by S-EOFs 4 and 5. It is dominated by wave-

numbers three and four, with some contribution of wavenumber five, and has both traveling and standing components. The S40 mode contributes only about 1.9% of IS variance in our SH data versus 4.0% for the S23 mode and 8.6% for the NH 40–50 day mode; by comparison, the tropical 40–50 day mode contributes about 3.0% of IS variance there.

A 16-day mode, while distinct from the previous two in SSA analysis, is too weak in order to isolate its spatial features by the techniques of compositing and Hovmöller diagrams which helped describe the 40-day and 23-day modes in greater detail. The tempting identification, by period alone, with the second antisymmetric Rossby mode of Laplace's tidal equation has already proved rather elusive (Mechoso and Hartmann 1982), and we hope to return to this problem in future work, by using some of the present results, as well as additional techniques beyond the scope of the present article. A mode with similar, 16–18 day period is also present, but equally weak, in the tropical and NH data.

Given the presence of three oscillating modes with similar frequencies in all three regions, the thought of global modes cannot be far away. Unfortunately, no significant correlations between leading T-PCs in the Southern Hemisphere, on the one hand, and in the tropics and Northern Hemisphere, on the other, could be found for any of the modes in the IS band. Time series of anomalies at key points identified by spatial EOF analysis in the SH data also failed to cross-correlate significantly with key points outside the Southern Hemisphere.

The two T-PCs of an oscillatory pair are in quadrature with each other at all times when the amplitude is sufficiently large. With this observation, the T-PCs allow one to follow the amplitude of each mode quite reliably through the seasons and from year to year. The 40-day mode is strongest in the winter season of either hemisphere. Considerable variability from year to year is apparent in all three modes (not shown here for the 23-day and 16-day modes), in both the timing of active intervals within the year and in the amplitude of the activity.

The IS variability of the Southern Hemisphere appears more complex than that of the Northern one in both spatial structure and temporal behavior. The variance spectrum of both S-EOFs and T-EOFs is flatter. Higher zonal wavenumbers—four, five and six—appear in the leading S-EOFs, while the leading NH EOFs are dominated by wavenumbers one-through-three. The temporal behavior, as represented by the SSA spectrum, indicates the presence of a larger number of degrees of freedom—about 300 versus the 120 found for NH data.

The cause of this greater complexity might be the less dominant role of forcing by topography (Kalnay et al. 1986), and the larger wavenumber of thermal surface anomalies—three rather than two. Still, the number of degrees of freedom of SH low-frequency variability does not exceed the number of variables of currently available, reasonably realistic nonlinear models of atmospheric flows on the sphere, whose behavior can be explored in considerable detail by the methods of modern nonlinear dynamics [see sections 6.4 and 6.5 of Ghil and Childress (1987), section 6b of Part I, and Ghil et al. (1991)].

Acknowledgments. It is a pleasure to thank two anonymous reviewers for their unusually detailed comments, and Isaac Held for suggesting to separate the SH results from the rest. This work was supported by NASA Grant NAG 5-713 and by NSF Grants ATM 86-15424 and ATM 90-13217. B. Gola, C. Monroe and C. Wong handled successive versions of the typescript on the word processor. K. Martelli and L. Lee helped prepare the figures for publication.

REFERENCES

Barnston, A. G., and R. E. Livezey, 1987: Classification, seasonality and persistence of low frequency atmospheric circulation patterns. *Mon. Wea. Rev.*, **115,** 1083–1126.

Branstator, G., 1987: A striking example of the atmosphere's leading traveling pattern. *J. Atmos. Sci.*, **44,** 2310–2323.

Broomhead, D. S., and G. P. King, 1986: Extracting qualitative dynamics from experimental data. *Physica,* **20D,** 217–236.

Farrara, J. D., M. Ghil, C. R. Mechoso and K. Mo, 1989: EOFs and multiple flow regimes in the Southern Hemisphere winter. *J. Atmos. Sci.*, **46,** 3219–3223.

Fraedrich, K., 1986: Estimating the dimensions of weather and climate attractors. *J. Atmos. Sci.*, **43,** 419–432.

Ghil, M., 1987: Dynamics, statistics and predictability of planetary flow regimes. *Irreversible Phenomena and Dynamical Systems Analysis in the Geosciences,* C. Nicolis and G. Nicolis, Eds., D. Reidel, 241–283.

——, 1988: The 1–2 month oscillation in the global atmosphere and nonlinear atmospheric dynamics. *Ann. Geophys.* (Special issue), 105–106.

——, and S. Childress, 1987: *Topics in Geophysical Fluid Dynamics: Atmospheric Dynamics, Dynamo Theory and Climate Dynamics,* Springer-Verlag, 485 pp.

——, and K. C. Mo, 1991: Intraseasonal oscillations in the global atmosphere. Part I: Northern Hemisphere and tropics. *J. Atmos. Sci.*, **48,** 752–779.

——, M. Kimoto and J. D. Neelin, 1991: Nonlinear dynamics and predictability in the atmospheric sciences. *Rev. Geophys.*, in press.

Hamilton, K., 1983: Aspects of wave behavior in the mid and upper troposphere of the Southern Hemisphere. *Atmos. Ocean,* **21,** 40–54.

Hartmann, D. L., 1977: Stationary planetary waves in the Southern Hemisphere. *J. Geophys. Res.*, **82,** 4930–4934.

Hovmöller, E., 1949: The trough-and-ridge diagram. *Tellus,* **1,** 62–66.

Jenkins, G. M., and D. G. Watts, 1968. *Spectral Analysis and its Applications.* Holden-Day, 525 pp.

Kalnay-Rivas, E., W. Baker, M. Halem, R. Atlas and D. Edelmann, 1981: GLAS experiments with FGGE II-b data. *Proc. Int. Conf. Preliminary FGGE Data Analysis Results,* Bergen, World Meteorological Organization, Geneva, 150–161.

Kalnay, E., K. C. Mo and J. Paegle, 1986: Large-amplitude, short-scale stationary Rossby waves in the Southern Hemisphere: Ob-

servations and mechanistic experiments to determine their origin. *J. Atmos. Sci.*, **43,** 252–275.

Knutson, T. R., and K. M. Weickmann, 1987: 30–60 day atmospheric oscillations: Composite life cycles of convection and circulation anomalies. *Mon. Wea. Rev.*, **115,** 1407–1436.

Kushnir, Y., 1987: Retrograding wintertime low-frequency disturbances over the North Pacific ocean. *J. Atmos. Sci.*, **44,** 2727–2742.

Mechoso, C. R., and D. L. Hartmann, 1982: An observational study of traveling planetary waves in the Southern Hemisphere. *J. Atmos. Sci.*, **39,** 1921–1935.

——, J. D. Farrara and M. Ghil, 1991: Intraseasonal variability of the winter circulation in the Southern Hemisphere atmosphere. *J. Atmos. Sci.*, in press.

Mo, K. C., 1986: Quasi-stationary states in the Southern Hemisphere. *Mon. Wea. Rev.*, **114,** 808–823.

——, and M. Ghil, 1987: Statistics and dynamics of persistent anomalies. *J. Atmos. Sci.*, **44,** 877–901.

Pike, E. R., J. G. McWhirter, M. Bertero and C. deMol, 1984: Generalized information theory for inverse problems in signal processing. *IEEE Proc.*, **131,** 660–667.

Randel, W. J., and J. L. Stanford, 1983: Structure of medium-scale atmospheric waves in the Southern Hemisphere summer. *J. Atmos. Sci.*, **40,** 2312–2318.

Rasmusson, E. M., X. Wang and C. F. Ropelewski, 1990: The biennial component of ENSO variability. *J. Mar. Sys.*, **1,** 71–96.

Salby, M. L., 1982: A ubiquitous wavenumber-5 anomaly in the Southern Hemisphere during FGGE. *Mon. Wea. Rev.*, **110,** 1712–1720.

Sciremammano, F., 1979: A suggestion for the presentation of correlations and their significance levels. *J. Phys. Oceanogr.*, **9,** 1273–1276.

Trenberth, K. E., 1985: Persistence of daily geopotential heights over the Southern Hemisphere. *Mon. Wea. Rev.*, **113,** 38–53.

——, and K. C. Mo, 1985: Blocking in the Southern Hemisphere. *Mon. Wea. Rev.*, **113,** 3–21.

Vautard, R., and M. Ghil, 1989: Singular spectrum analysis in nonlinear dynamics, with applications to paleoclimatic time series. *Physica,* **35D,** 395–424.

——, K. C. Mo and M. Ghil, 1990: Statistical significance test for transition matrices of atmospheric Markov chains. *J. Atmos. Sci.*, **47,** 1926–1931.